Complex-Envelope ADE-LOD-FDTD for Band Gap Analysis of Plasma Photonic Crystals

Tu-Lu Liang, Wei Shao, and Sheng-Bing Shi

School of Physics
University of Electronic Science and Technology of China, Chengdu, 610054, China
liangtul@163.com, weishao@uestc.edu.cn, shengbing77@163.com

Abstract ─ In this paper, a complex-envelope (CE) scheme is introduced into the locally one-dimensional finite-difference time-domain (LOD-FDTD) method for the band-gap analysis of the plasma photonic crystal (PPC). The un-magnetized plasma, characterized by a complex frequency-dependent permittivity, is expressed by the Drude model and solved with a generalized auxiliary differential equation (ADE) technique. The CE scheme is also applied to the perfectly matched layer. Numerical examples show that the proposed CE-ADE-LOD-FDTD method provides much more accurate results than the traditional ADE-LOD-FDTD with the same CFL number. The reflection and transmission coefficients of the PPC are calculated and their dependence on the relative permittivity of dielectric, the plasma frequency, the collision frequency and the plasma layer thickness is studied. The results show that the photonic band gaps of the PPC could be tuned by adjusting the parameters.

Index Terms ─ Band-gaps, complex envelope (CE), locally one-dimensional finite-difference time-domain (LOD-FDTD) method, plasma photonic crystal (PPC).

I. INTRODUCTION

Much attention has been paid to the photonic crystal due to its unique characteristics since the conception was put forward by Yablonovitch [1] and John [2] in the 1980s. The plasma photonic crystal (PPC) is an important branch of the photonic crystal. A PPC structure is an artificially periodic one composed of the alternating thin un-magnetized (or magnetized) plasmas and dielectric materials (or vacuum). In recent years, scholars have devoted much of the energy to the research of PPCs. At the same time, a number of related literatures continue to emerge. The natures of the PPC include photonic band gap properties of photonic localization and optical properties [3], [4]. For the analysis of the PPC, the frequency-dependent finite-difference time-domain (FDTD) method has been widely used. Because surface plasmon polaritons (SPPs) are highly localized along the plasma-dielectric interface, fine spatial grids are required to attain sufficient accuracy. Thus, an extremely small time step constrained by the Courant-Friedrich-Levy (CFL) stability condition results in a long computation time [5].

Some unconditionally stable FDTD methods have been presented to eliminate the CFL condition and to improve the computational efficiency. Several unconditionally stable time-marching methods only need to deal with the tri-diagonal matrix equation with low computational complexity, such as the locally one-dimensional (LOD) FDTD method [6], [7], the alternating-direction implicit (ADI) FDTD method [8], [9] and the split-step (SS) FDTD method [10]-[12]. The unconditionally stable Crank-Nicolson (CN) FDTD method is another time-marching method, in which the full time step size in one marching step is used to solve the discretized Maxwell's equations [13], [14]. Although the above time-marching methods are unconditionally stable, their time steps are restricted by the dispersion errors [15]-[17]. The order-marching weighted Laguerre polynomial (WLP) FDTD method, in which the spatial and the temporal variables are separated, does not have to deal with the time step [18], [19]. Both CN-FDTD and WLP-FDTD have to solve a large banded-spare matrix equation at the beginning of the calculation.

In order to reduce the numerical dispersion for large time-step sizes in ADI-FDTD, a technique called the complex-envelope (CE) has been proposed in [20]. It was claimed that CE-ADI-FDTD is more accurate than ADI-FDTD with the same time step. By using the CE technique, the carrier frequency term is absorbed into the Maxwell's equations as a known quantity. Consequently, only the signal envelopes become the variants to be sampled and computed. Generally, LOD-FDTD requires fewer arithmetic operations than ADI-FDTD [21]. [22] introduced a CE-LOD-FDTD method for the analysis of the optical waveguide. The CE-LOD-FDTD method was also used to analyze ionospheric propagation in a simple one-dimensional space without absorbing boundary conditions [23].

With the auxiliary differential equation (ADE) technique [24], [25], the CE-LOD-FDTD method is employed for the analysis of PPCs in this work. The

Submitted On: July 28, 2017
Accepted On: April 21, 2018

dispersion of the plasma expressed by the Drude model, is solved with the ADE technique to establish the relationship between the electric field intensity and conductive electric current in the PPC. Furthermore, the CE technique is integrated with the Berenger's perfectly matched layer (PML) to truncate the computational domain effectively. With the proposed CE-ADE-LOD-FDTD method, the reflection and transmission coefficients through the PPC are calculated, and their dependence on the dielectric permittivity, the plasma frequency, the collision frequency and the plasma layer thickness is studied. The numerical examples verify accuracy and effectiveness of the proposed method.

II. NUMERICAL FORMULATION

A. CE-ADE-LOD-FDTD method

The time dependence of $e^{-i\omega t}$ is assumed. According to the Drude model, the relative permittivity (in frequency domain) of the un-magnetized plasma is given by:

$$\varepsilon_{\mathrm{m}}(\omega)=1-\frac{\omega_{\mathrm{p}}^2}{\omega^2+\mathrm{i}\gamma\omega}, \tag{1}$$

where ω is the angular frequency of the impinging light, ω_{p} is the plasma frequency, and γ is the collision frequency of the plasma.

For simplicity, a 2-D TM wave including E_x, E_z and H_y components is considered. The 2-D Maxwell's equations and auxiliary differential equations in a dispersive material can be written as [26]:

$$\frac{\partial E_x}{\partial t}=-\frac{1}{\varepsilon}\frac{\partial H_y}{\partial z}-\frac{1}{\varepsilon}J_x, \tag{2a}$$

$$\frac{\partial E_z}{\partial t}=\frac{1}{\varepsilon}\frac{\partial H_y}{\partial x}-\frac{1}{\varepsilon}J_z, \tag{2b}$$

$$\frac{\partial H_y}{\partial t}=\frac{1}{\mu_0}\frac{\partial E_z}{\partial x}-\frac{1}{\mu_0}\frac{\partial E_x}{\partial z}, \tag{2c}$$

$$\frac{\partial J_x}{\partial t}=-\gamma J_x+\varepsilon_0\omega_{\mathrm{p}}^2E_x, \tag{2d}$$

$$\frac{\partial J_z}{\partial t}=-\gamma J_z+\varepsilon_0\omega_{\mathrm{p}}^2E_z, \tag{2e}$$

where ε and ε_0 are the electric permittivity of the medium and free space, respectively, and μ_0 is the magnetic permeability.

The fields can be represented as:

$$(E,H,J)=\mathrm{Re}\left\{\left(\hat{E},\hat{H},\hat{J}\right)e^{\mathrm{i}\omega_{\mathrm{c}}t}\right\}, \tag{3}$$

where Re{·} denotes the operation that takes the real part of a complex number, ω_{c} is the center carrier angular frequency, and $\hat{E}$, $\hat{H}$ and $\hat{J}$ represent the associated complex-envelope fields and electric current.

Substituting (3) into (2a)-(2e), we get:

$$\frac{\partial\hat{E}_x}{\partial t}+\mathrm{i}\omega_{\mathrm{c}}\hat{E}_x=-\frac{1}{\varepsilon}\frac{\partial\hat{H}_y}{\partial z}-\frac{1}{\varepsilon}\hat{J}_x, \tag{4a}$$

$$\frac{\partial\hat{E}_z}{\partial t}+\mathrm{i}\omega_{\mathrm{c}}\hat{E}_z=\frac{1}{\varepsilon}\frac{\partial\hat{H}_y}{\partial x}-\frac{1}{\varepsilon}\hat{J}_z, \tag{4b}$$

$$\frac{\partial\hat{H}_y}{\partial t}+\mathrm{i}\omega_{\mathrm{c}}\hat{H}_y=\frac{1}{\mu_0}\frac{\partial\hat{E}_z}{\partial x}-\frac{1}{\mu_0}\frac{\partial\hat{E}_x}{\partial z}, \tag{4c}$$

$$\frac{\partial\hat{J}_x}{\partial t}+\mathrm{i}\omega_{\mathrm{c}}\hat{J}_x=-\gamma\hat{J}_x+\varepsilon_0\omega_{\mathrm{p}}^2\hat{E}_x, \tag{4d}$$

$$\frac{\partial\hat{J}_z}{\partial t}+\mathrm{i}\omega_{\mathrm{c}}\hat{J}_z=-\gamma\hat{J}_z+\varepsilon_0\omega_{\mathrm{p}}^2\hat{E}_z. \tag{4e}$$

With the LOD scheme [6], we obtain the CE-ADE-LOD-FDTD formalism. In the first step (n+1/2), we have:

$$\hat{E}_x^{n+1/2}=\frac{4-\mathrm{i}\omega_{\mathrm{c}}\Delta t}{4+\mathrm{i}\omega_{\mathrm{c}}\Delta t}\hat{E}_x^n, \tag{5a}$$

$$\hat{E}_z^{n+1/2}=\frac{4-\mathrm{i}\omega_{\mathrm{c}}\Delta t}{4+\mathrm{i}\omega_{\mathrm{c}}\Delta t}\hat{E}_z^n+\frac{2\Delta t}{4\varepsilon+\mathrm{i}\omega_{\mathrm{c}}\varepsilon\Delta t}\left(\frac{\partial\hat{H}_y^{n+1/2}}{\partial x}+\frac{\partial\hat{H}_y^{n}}{\partial x}-\hat{J}_z^{n+1/2}-\hat{J}_z^{n}\right), \tag{5b}$$

$$\hat{H}_y^{n+1/2}=\frac{4-\mathrm{i}\omega_{\mathrm{c}}\Delta t}{4+\mathrm{i}\omega_{\mathrm{c}}\Delta t}\hat{H}_y^n+\frac{2\Delta t}{4\mu_0+\mathrm{i}\omega_{\mathrm{c}}\mu_0\Delta t}\left(\frac{\partial\hat{E}_z^{n+1/2}}{\partial x}+\frac{\partial\hat{E}_z^{n}}{\partial x}\right), \tag{5c}$$

$$\hat{J}_x^{n+1/2}=\frac{4-\mathrm{i}\omega_{\mathrm{c}}\Delta t-2\gamma\Delta t}{4+\mathrm{i}\omega_{\mathrm{c}}\Delta t+2\gamma\Delta t}\hat{J}_x^n+\frac{2\varepsilon_0\omega_{\mathrm{p}}^2\Delta t}{4+\mathrm{i}\omega_{\mathrm{c}}\Delta t+2\gamma\Delta t}\left(\hat{E}_x^{n+1/2}+\hat{E}_x^{n}\right), \tag{5d}$$

$$\hat{J}_z^{n+1/2}=\frac{4-\mathrm{i}\omega_{\mathrm{c}}\Delta t}{4+\mathrm{i}\omega_{\mathrm{c}}\Delta t}\hat{J}_z^n. \tag{5e}$$

In the second step (n+1), we have:

$$\hat{E}_x^{n+1}=\frac{4-\mathrm{i}\omega_{\mathrm{c}}\Delta t}{4+\mathrm{i}\omega_{\mathrm{c}}\Delta t}\hat{E}_x^{n+1/2}-\frac{2\Delta t}{4\varepsilon+\mathrm{i}\omega_{\mathrm{c}}\varepsilon\Delta t}\left(\frac{\partial\hat{H}_y^{n+1}}{\partial z}+\frac{\partial\hat{H}_y^{n+1/2}}{\partial z}+\hat{J}_x^{n+1}+\hat{J}_x^{n+1/2}\right), \tag{6a}$$

$$\hat{E}_z^{n+1}=\frac{4-\mathrm{i}\omega_{\mathrm{c}}\Delta t}{4+\mathrm{i}\omega_{\mathrm{c}}\Delta t}\hat{E}_z^{n+1/2}, \tag{6b}$$

$$\hat{H}_y^{n+1}=\frac{4-\mathrm{i}\omega_{\mathrm{c}}\Delta t}{4+\mathrm{i}\omega_{\mathrm{c}}\Delta t}\hat{H}_y^{n+1/2}-\frac{2\Delta t}{4\mu_0+\mathrm{i}\omega_{\mathrm{c}}\mu_0\Delta t}\left(\frac{\partial\hat{E}_x^{n+1}}{\partial z}+\frac{\partial\hat{E}_x^{n+1/2}}{\partial z}\right), \tag{6c}$$

$$\hat{J}_x^{n+1}=\frac{4-\mathrm{i}\omega_{\mathrm{c}}\Delta t}{4+\mathrm{i}\omega_{\mathrm{c}}\Delta t}\hat{J}_x^{n+1/2}, \tag{6d}$$

$$\hat{J}_z^{n+1}=\frac{4-\mathrm{i}\omega_{\mathrm{c}}\Delta t-2\gamma\Delta t}{4+\mathrm{i}\omega_{\mathrm{c}}\Delta t+2\gamma\Delta t}\hat{J}_z^{n+1/2}+\frac{2\varepsilon_0\omega_{\mathrm{p}}^2\Delta t}{4+\mathrm{i}\omega_{\mathrm{c}}\Delta t+2\gamma\Delta t}\left(\hat{E}_z^{n+1}+\hat{E}_z^{n+1/2}\right). \tag{6e}$$

Since (5b) includes the unknown term $\hat{H}_y^{n+1/2}$, taking the first step for example, we substitute (5c) into (5b) to eliminate $\hat{H}_y^{n+1/2}$ and then get a tri-diagonal matrix equation in term of $\hat{E}_z^{n+1/2}$ which can be solved with Thomas algorithm. The rest of the equations can be calculated in an explicit way. It is clear that the equations of the CE-ADE-LOD-FDTD method degrade into those of the ADE-LOD-FDTD method for $\omega_c = 0$.

B. CE-PML in CE-ADE-LOD-FDTD

In a Berenger's PML medium, the magnetic field component $\hat{H}_y$ is divided into $\hat{H}_{yx}$ and $\hat{H}_{yz}$. With the LOD scheme [6], we obtain the CE-PML difference formalism in the first step (n+1/2):

$$\hat{E}_x^{n+1/2}\big|_{i+1/2,k} = A\hat{E}_x^{n}\big|_{i+1/2,k}\,, \tag{7a}$$

$$\begin{aligned}\hat{E}_z^{n+1/2}\big|_{i,k+1/2} &= C_1\big|_{i,k+1/2}\,\hat{E}_z^{n}\big|_{i,k+1/2} \\ &+ C_2\big|_{i,k+1/2}\left(\hat{H}_{yx}^{n+1/2}\big|_{i+1/2,k+1/2} - \hat{H}_{yx}^{n+1/2}\big|_{i-1/2,k+1/2}\right) \\ &+ C_2\big|_{i,k+1/2}\left(\hat{H}_{yx}^{n}\big|_{i+1/2,k+1/2} - \hat{H}_{yx}^{n}\big|_{i-1/2,k+1/2}\right) \\ &+ C_2\big|_{i,k+1/2}\begin{pmatrix}\hat{H}_{yz}^{n+1/2}\big|_{i+1/2,k+1/2} - \hat{H}_{yz}^{n+1/2}\big|_{i-1/2,k+1/2} \\ +\hat{H}_{yz}^{n}\big|_{i+1/2,k+1/2} - \hat{H}_{yz}^{n}\big|_{i-1/2,k+1/2}\end{pmatrix}, \\ &- \frac{\Delta x_i + \Delta x_{i-1}}{2}\cdot C_2\big|_{i,k+1/2}\left(\hat{J}_z^{n+1/2}\big|_{i,k+1/2} + \hat{J}_z^{n}\big|_{i,k+1/2}\right)\end{aligned} \tag{7b}$$

$$\begin{aligned}\hat{H}_{yx}^{n+1/2}\big|_{i+1/2,k+1/2} &= C_3\big|_{i+1/2}\,\hat{H}_{yx}^{n}\big|_{i+1/2,k+1/2} \\ &+ C_4\big|_{i+1/2}\begin{pmatrix}\hat{E}_z^{n+1/2}\big|_{i+1,k+1/2} - \hat{E}_z^{n+1/2}\big|_{i,k+1/2} \\ +\hat{E}_z^{n}\big|_{i+1,k+1/2} - \hat{E}_z^{n}\big|_{i,k+1/2}\end{pmatrix},\end{aligned} \tag{7c}$$

$$\hat{H}_{yz}^{n+1/2}\big|_{i+1/2,k+1/2} = A\hat{H}_{yz}^{n}\big|_{i+1/2,k+1/2}\,, \tag{7d}$$

$$\begin{aligned}\hat{J}_x^{n+1/2}\big|_{i+1/2,k} &= \frac{2-\mathrm{i}\omega_c\Delta t/2-\Delta t\gamma\big|_{i+1/2,k}}{2+\mathrm{i}\omega_c\Delta t/2+\Delta t\gamma\big|_{i+1/2,k}}\,\hat{J}_x^{n}\big|_{i+1/2,k} \\ &+ \frac{\varepsilon_0\Delta t\omega_p^2\big|_{i+1/2,k}}{2+\mathrm{i}\omega_c\Delta t/2+\Delta t\gamma\big|_{i+1/2,k}}\left(\hat{E}_x^{n+1/2}\big|_{i+1/2,k} + \hat{E}_x^{n}\big|_{i+1/2,k}\right),\end{aligned} \tag{7e}$$

$$\hat{J}_z^{n+1/2}\big|_{i,k+1/2} = A\hat{J}_z^{n}\big|_{i,k+1/2}\,. \tag{7f}$$

The coefficients of (7a)–(7f) are expressed as:

$$A = \frac{4-\mathrm{i}\omega_c\Delta t}{4+\mathrm{i}\omega_c\Delta t}\,, \tag{8a}$$

$$C_1\big|_{i,k+1/2} = \frac{2\varepsilon\big|_{i,k+1/2} - \mathrm{i}\omega_c\varepsilon_0\Delta t/2 - \Delta t\sigma_x\big|_i}{2\varepsilon\big|_{i,k+1/2} + \mathrm{i}\omega_c\varepsilon_0\Delta t/2 + \Delta t\sigma_x\big|_i}\,, \tag{8b}$$

$$C_2\big|_{i,k+1/2} = \frac{2\Delta t}{\left(2\varepsilon\big|_{i,k+1/2} + \mathrm{i}\omega_c\varepsilon_0\Delta t/2 + \Delta t\sigma_x\big|_i\right)\left(\Delta x_i + \Delta x_{i-1}\right)}\,, \tag{8c}$$

$$C_3\big|_{i+1/2} = \frac{2\mu_0 - \mathrm{i}\omega_c\mu_0\Delta t/2 - \Delta t\rho_x\big|_{i+1/2}}{2\mu_0 + \mathrm{i}\omega_c\mu_0\Delta t/2 + \Delta t\rho_x\big|_{i+1/2}}\,, \tag{8d}$$

$$C_4\big|_{i+1/2} = \frac{\Delta t}{\left(2\mu_0 + \mathrm{i}\omega_c\mu_0\Delta t/2 + \Delta t\rho_x\big|_{i+1/2}\right)\Delta x_i}\,, \tag{8e}$$

where Δt is the time step, Δx_i is the discretization step along the x-direction, σ_x and ρ_x are the conductivity and reluctivity, respectively. The equations of the second step can be obtained in a similar way.

III. NUMERICAL RESULTS AND DISCUSSION

With the proposed CE-ADE-LOD-FDTD method, the reflection and transmission coefficients through the PPC are calculated and their dependence on the relative permittivity of dielectric medium, the plasma frequency, the plasma collision frequency and the plasma layer thickness is studied in this section.

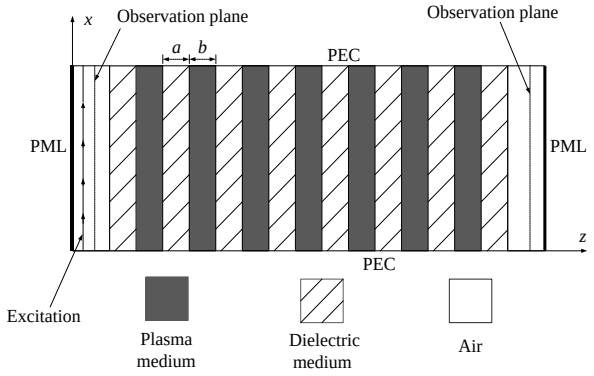

Fig. 1. Schematic model of a plasma photonic crystal.

A normally incident TM-polarized plane wave illuminates a PPC from the left side, as shown in Fig. 1. The eight dielectric layers and seven plasma layers are set in the PPC model, where $a = b = 15$ μm. The computational region is truncated by the Berenger's PML on the left and right sides. The top and bottom boundaries are treated by the perfect electric conductors (PECs).

A Gaussian pulse is used as the source excitation, which can be written as:

$$F(t) = e^{-\frac{(t-t_0)^2}{\tau^2}}\,, \tag{9}$$

where the maximum frequency $f_{max} = 10$ THz, $\tau = 1/(2f_{max})$ and $t_0 = 3\tau$. The frequency characteristics of the transmission are calculated with the discrete Fourier transform (DFT) of time-domain responses in the observation plane.

Here, the graded cells are used to attain sufficient accuracy. The center carrier angular frequency $\omega_c = 2\pi \times 5 \times 10^{12}$ rad/s, the spatial step along the x-direction is 1.5 μm, and the minimum and maximum spatial steps

along the *z*-direction are Δ_{min} = 0.05 μm and Δ_{max} = 2 μm, respectively. The total cell number in the computational domain is 40 × 355.

A. Accuracy verification of CE-ADE-LOD-FDTD

First, the accuracy and effectiveness of the proposed CE-ADE-LOD-FDTD method are verified. We choose the plasma frequency $\omega_p = 2\pi \times 2 \times 10^{12}$ rad/s, the plasma collision frequency γ = 40 THz, and the relative permittivity of dielectric ε_r = 4 in the simulation.

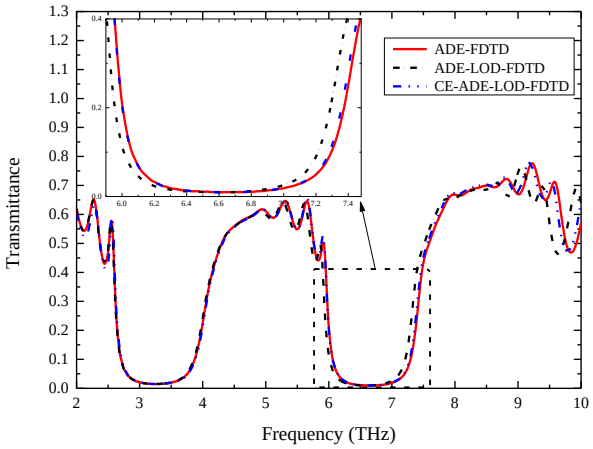

Fig. 2. Results of transmittance of the PPC from ADE-FDTD, ADE-LOD-FDTD and CE-ADE-LOD-FDTD.

Table 1: Comparison of the computational efforts for the three methods

Method	CFLN	Marching Steps	CPU Time (s)	Memory (Mb)
FDTD	1	200000	45017	8.99
ADE-LOD-FDTD	100	2000	251	11.35
CE-ADE-LOD-FDTD	100	2000	529	16.06

Figure 2 shows the transmission coefficients calculated by ADE-FDTD, ADE-LOD-FDTD [26], and the proposed CE-ADE-LOD-FDTD method, where $\Delta t_{FDTD} = \Delta_{min}/2/c$ (c is the velocity of light in the vacuum) is chosen for the explicit ADE-FDTD according to the CFL constraint, $\Delta t_{LOD} = 100\Delta t_{FDTD}$ (CFLN = Δt_{LOD} /Δt_{FDTD} = 100) is chosen for ADE-LOD-FDTD, and $\Delta t_{CE\text{-}LOD} = 100\Delta t_{FDTD}$ (CFLN = 100) is chosen for CE-ADE-LOD-FDTD. It is clear from Fig. 2 that the results from CE-ADE-LOD-FDTD and ADE-FDTD are in good agreement. The results from ADE-LOD-FDTD are worse than those from the other two methods because its dispersion deteriorates with the large time step.

Table 1 shows the comparison of computational efforts of the three methods. Because of the storage of the sparse matrix, the memory requirement of CE-ADE-LOD-FDTD is larger than ADE-FDTD. With the much larger time step beyond the CFL constraint, the CPU time of CE-ADE-LOD-FDTD can be much less than that of ADE-FDTD. Although CE-ADE-LOD-FDTD costs more CPU time than ADE-LOD-FDTD, it gets much more accuracy results. All calculations in this paper are performed on an AMD Athlon (tm) II X4 3.00 GHz computer with 6 GB RAM.

B. Effects of the relative permittivity of dielectric

First, we discuss the effects of the relative permittivity of dielectric on the band gap of the PPC. We choose the plasma frequency $\omega_p = 2\pi \times 2 \times 10^{12}$ rad/s and the plasma collision frequency γ = 40 THz in the simulation. With the proposed CE-ADE-LOD-FDTD method, the reflection and transmission coefficients for the PPC with different relative permittivities of dielectric are depicted in Figs. 3, 4 and 5. Here, we choose CFLN = 100 in the CE-ADE-LOD-FDTD method.

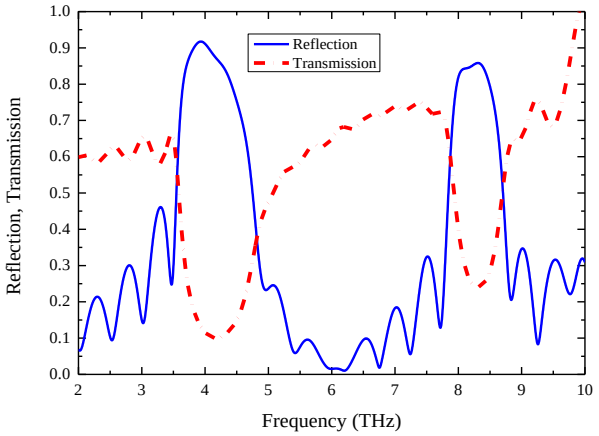

Fig. 3. Electromagnetic band-gap characteristics with the relative dielectric permittivity ε_r = 2.

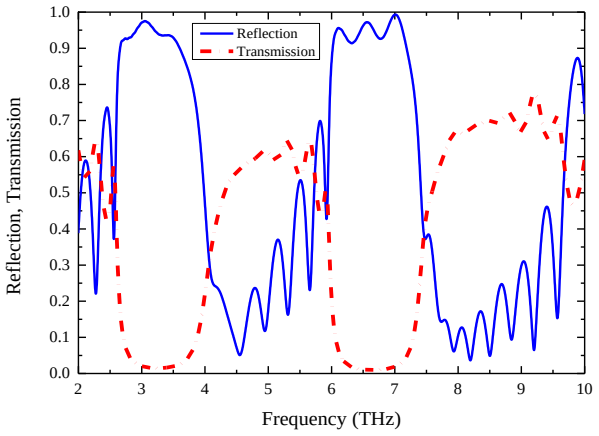

Fig. 4. Electromagnetic band-gap characteristics with the relative dielectric permittivity ε_r = 4.

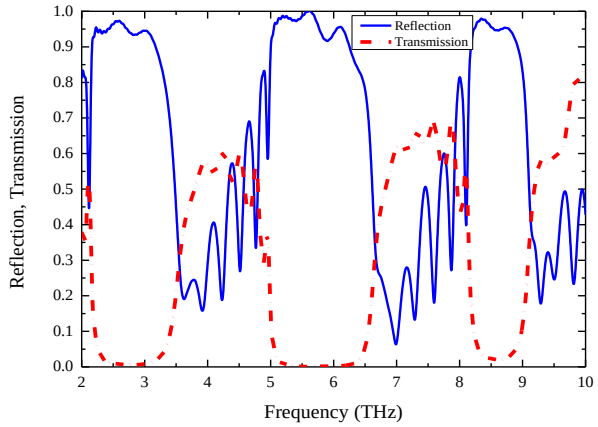

Fig. 5. Electromagnetic band-gap characteristics with the relative dielectric permittivity $\varepsilon_r = 6$.

It is difficult to form the band gap when the relative permittivity of the dielectric medium equals to 1 because the dielectric constant of the plasma is close to 1. That means that the PPC structure tends to a single medium when the relative permittivity of the dielectric medium is close to that of the background medium. The double band gap appears near $f = 4.2$ THz and 8.4 THz when the relative permittivity of the dielectric medium equals to 2. With the increase of the relative permittivity value of the dielectric medium, the depth and number of the band gap increase. Therefore, the band gap can be well controlled by changing the relative permittivity value of the dielectric medium.

C. Effects of the plasma frequency

Next, we study the effects of the plasma frequency on the band gap of the PPC. Here we choose the relative permittivity of the dielectric medium $\varepsilon_r = 5$, and the plasma collision frequency $\gamma = 40$ THz in the simulation. Figure 6 depicts the transmission coefficients for the plasma frequency from $\omega_p = 2\pi \times 2 \times 10^{12}$ rad/s to $2\pi \times 10 \times 10^{12}$ rad/s.

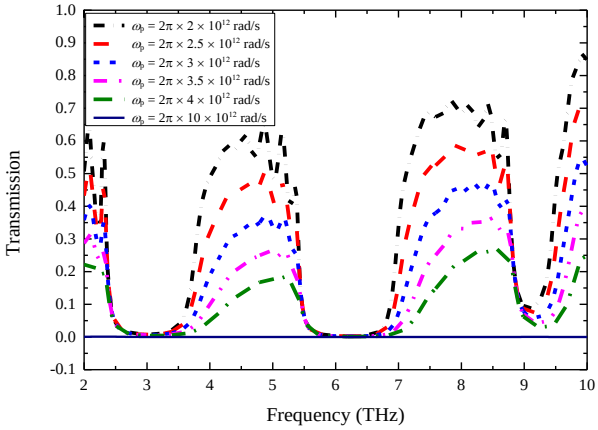

Fig. 6. Transmittance of different plasma frequencies.

With the increase of the plasma frequency, from Fig. 6, the periodicity of photonic band gaps gets unobvious, but the band gap range is a little extended. The transmission coefficient of the PPC will be reduced to zero when the plasma frequency increases to a certain value. This is mainly because when the frequency of the incident electromagnetic wave is close to the maximum plasma frequency, the attenuation of the electromagnetic wave becomes very large, i.e., the resonance attenuation [27].

D. Effects of the Plasma Collision Frequency

Then, we discuss the effects of the plasma collision frequency on the band gap of the PPC. Here we choose the relative permittivity of the dielectric medium $\varepsilon_r = 5$ and the plasma frequency $\omega_p = 2\pi \times 2 \times 10^{12}$ rad/s in the simulation. Figure 7 depicts the transmission coefficients for the plasma collision frequency from $\gamma = 20$ THz to 80 THz. From Fig. 7, the plasma collision frequency has little effect on the periodicity of the band gap.

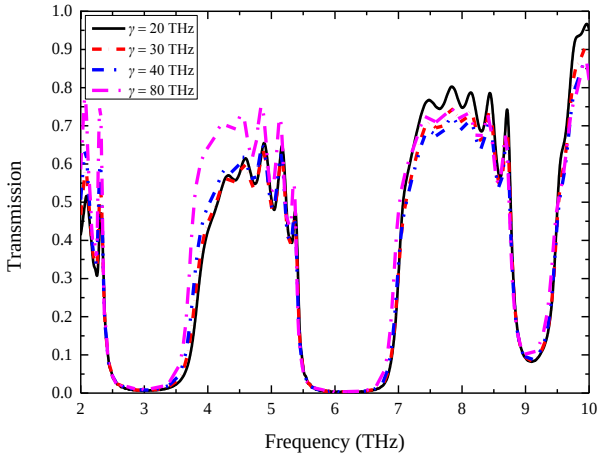

Fig. 7. Transmittance of different plasma collision frequencies.

E. Effects of the plasma layer thickness

Finally, we study the effects of the variation of the plasma layer thickness on the band gap of the PPC. Here we choose the relative permittivity of the dielectric medium $\varepsilon_r = 4$, the plasma frequency $\omega_p = 2\pi \times 2 \times 10^{12}$ rad/s, and the plasma collision frequency $\gamma = 40$ THz in the simulation. Figure 8 depicts the transmission coefficients for the plasma layer thickness from $b = 15$ μm to 49 μm. From Fig. 8, with the increase of the plasma layer thickness, the periodicity of the band gap deteriorates. The absorption performance of the plasma enhances with the increase of plasma layer thickness, and then the attenuation of the incident wave gets large. The periodic band gaps can be generated when the frequency of the incident wave is high and the plasma layer thickness is small.

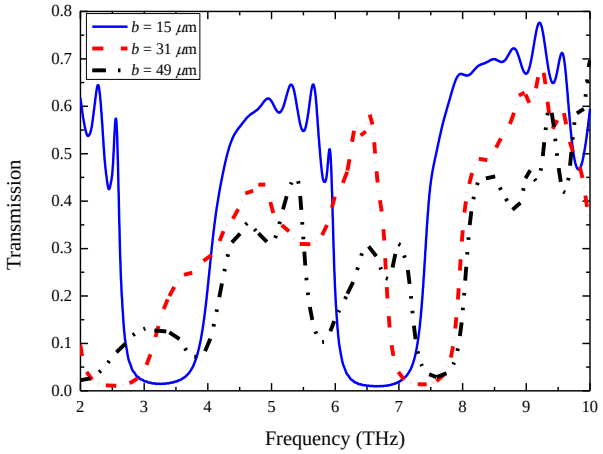

Fig. 8. Transmittance of different plasma layer thicknesses.

IV. CONCLUSION

In this paper, an effective time-domain method with Berenger's PML has been developed for the analysis of the band-gap characteristics in the PPC. With the introduction of the CE technique, the ADE-LOD-FDTD method can provide much more accurate results than the traditional ADE-LOD-FDTD in the numerical examples. The numerical examples verify accuracy and effectiveness of the proposed method, and the results show that the photonic band gaps of the PPC could be tuned by changing the value of the relative permittivity of the dielectric medium, the plasma frequency or the plasma layer thickness.

ACKNOWLEDGMENT

This work was supported by the National Natural Science Foundation of China (61471105 and 61331007) and 973 Project (No. 613273).

REFERENCES

[1] E. Yablonovitch, "Inhibited spontaneous emission in solid-state physics and electronics," *Phys. Rev. Lett.*, vol. 58, no. 20, pp. 2059-2062, May 1987.

[2] S. John, "Strong localization of photons in certain disordered dielectric superlattices," *Phys. Rev. Lett.*, vol. 58, no. 23, pp. 2486-2489, June 1987.

[3] J. G. Fleming and S. Y. Lin, "Three-dimensional photonic crystal with a stop band from 1.35 to 1.95 μm," *Opt. Lett.*, vol. 24, no. 1, pp. 49-51, Jan. 1999.

[4] S. Noda, K. Tomoda, N. Yamanoto, and A. Chutinan, "Full three-dimensional photonic band gap crystals at near-infrared wavelengths," *Science*, vol. no. 5479, pp. 604-606, July 2000.

[5] A. Taflove and S. C. Hagness, *Computational Electro-dynamics: The Finite-Difference Time-Domain Method*. Norwood, MA: Artech House, 2000.

[6] J. Shibayama, M. Muraki, J. Yamauchi, and H. Nakano, "Efficient implicit FDTD algorithm based on locally one-dimensional scheme," *Electron. Lett.*, vol. 41, no. 19, pp. 1046-1047, Sep. 2005.

[7] V. E. D. Nascimento, B.-H. V. Borges, and F. L. Teixeira, "Split-field PML implementations for the unconditionally stable LOD-FDTD method," *IEEE Microw. Wireless Compon. Lett.*, vol. 16, no. 7, pp. 398-400, July 2006.

[8] T. Namiki, "A new FDTD algorithm based on alternating-direction implicit method," *IEEE Trans. Microw. Theory Tech.*, vol. 47, no. 10, pp. 2003-2007, Oct. 1999.

[9] F. H. Zheng, Z. Z. Chen, and J. Z. Zhang, "A finite-difference time-domain method without the Courant stability conditions," *IEEE Microw. Guided Wave Lett.*, vol. 9, no. 11, pp. 441-443, Nov. 1999.

[10] J. Lee and B. Fornberg, "A split step approach for the 3-D maxwell's equations," *J. Comput. Appl. Math.*, vol. 158, no. 5, pp. 485-505, Sep. 2003.

[11] J. Lee and B. Fornberg, "Some unconditionally stable time stepping methods for the 3-D Maxwell's equations," *J. Comput. Appl. Math.*, vol. 166, no. 2, pp. 497-523, Apr. 2004.

[12] L. Gao, B. Zhang, and D. Liang, "The splitting finite difference time-domain methods for Maxwell's equations in two dimensions," *J. Comput. Appl. Math.*, vol. 205, no. 1, pp. 207-230, Aug. 2007.

[13] G. Sun and C. W. Trueman, "Approximate Crank-Nicolson schemes for the 2-D finite-difference time-domain method for TE_z waves," *IEEE Trans. Antennas Propag.*, vol. 52, no. 11, pp. 2963-2972, Nov. 2004.

[14] G. Sun and C. W. Truneman, "Efficient implementations of the Crank-Nicolson scheme for the finite-difference time-domain method," *IEEE Trans. Microw. Theory Tech.*, vol. 54, no. 5, pp. 2275-2284, May 2006.

[15] J. Lee and B. Fornberg, "A split step approach for the 3-D maxwell's equations," *J. Comput. Appl. Math.*, vol. 158, no. 5, pp. 485-505, Sep. 2003.

[16] F. Zheng and Z. Chen, "Numerical dispersion analysis of the unconditionally stable 3-D ADI-FDTD method," *IEEE Trans. Microw. Theory Tech.*, vol. 49, no. 5, pp. 1006-1009, May 2001.

[17] I. Ahmed, E. K. Chun, and E. P. Li, "Numerical dispersion analysis of the unconditionally stable three-dimensional LOD-FDTD method," *IEEE Trans. Antennas Propag.*, vol. 58, no. 12, pp. 3983-3989, Dec. 2010.

[18] Y. S. Chung, T. K. Sarkar, B. H. Jung, and M. Salazar-Palma, "An unconditionally stable scheme for the finite-difference time-domain method," *IEEE Trans. Microw. Theory Tech.*, vol. 51, no. 3,

pp. 697-704, Mar. 2003.
[19] M. Ha, K. Srinivasan, and M. Swaminathan, "Transient chip-package co-simulation using the Laguerre-FDTD scheme," *IEEE Trans. Adv. Packag.*, vol. 32, no. 4, pp. 816-830, Nov. 2009.
[20] H. Rao, R. Scarmozzino, and R. M. Osgood, "An improved ADI-FDTD method and its application to photonic simulations," *IEEE Photon. Technol. Lett.*, vol. 14, no. 4, pp. 477-479, Apr. 2002.
[21] I. Ahmed, E. K. Chua, E. P. Li, and Z. Z. Chen, "Development of the three-dimensional unconditionally stable LOD-FDTD method," *IEEE Trans. Antennas Propag*., vol. 56, no. 11, pp. 3596-3600, Nov. 2008.
[22] J. Shibayama, M. Muraki, R. Takahashi, J. Yamauchi, and H. Nakano, "Performance evaluation of several implicit FDTD methods for optical waveguide analyses," *J. Lightw. Technol.*, vol. 24, no. 6, pp. 2465-2472, June 2006.
[23] D. Y. Heh and E. L. Tan, "Complex-envelope LOD-FDTD method for ionospheric propagation," in *IEEE International Symposium on Antennas and Propagation (APSURSI)*, Fajardo, pp. 2027-2028, 2016.
[24] S. K. Gray and T. Kupka, "Propagation of light in metallic nanowire arrays: Finite-difference time-domain studies of silver cylinders," *Physical Review B.*, vol. 68, no. 4, pp. 045415, July 2003.
[25] J. Shibayama, R. Takahashi, J. Yamauchi, and H. Nakano, "Frequency-dependent LOD-FDTD implementtations for dispersive media," *Electron. Lett.*, vol. 42, no. 19, pp. 1084-1086, Sep. 2006.
[26] T. L. Liang, W. Shao, S. B. Shi, and H. Ou, "Analysis of extraordinary optical transmission with periodic metallic gratings using ADE-LOD-FDTD method," *IEEE Photon. J.*, vol. 8, no. 5, pp. 7804710, Oct. 2016.
[27] N. C. Panoiu, R. M. Osgood, S. Zhang, and S. R. J. Brueck, "Zero-*n* bandgap in photonic crystal superlattices," *J. Opt. Soc. Am. B.*, vol. 23, no. 3, pp. 506-513, Mar. 2006.

Tu-Lu Liang was born in Jiangxi, China, in 1991. He received the B.S. degree in Physics from the GanNan Normal University, Ganzhou, China, in 2014. Currently, he is working toward the Ph.D. degree in Radio Physics at the University of Electronic Science and Technology of China (UESTC), Chengdu, China.

His research interest is computational electromagnetic.

Wei Shao received the B.E. degree in Electrical Engineering, and the M.Sc. and Ph.D. degrees in Radio Physics from the University of Electronic Science and Technology of China (UESTC), Chengdu, in 1998, 2004, and 2006, respectively. He joined the UESTC in 2007. From 2010 to 2011, he was a Visiting Scholar with the Electromagnetic Communication Laboratory, Pennsylvania State University, State College, PA, USA. He is currently a Professor with UESTC.

His current research interests include computational electromagnetics and antenna design.

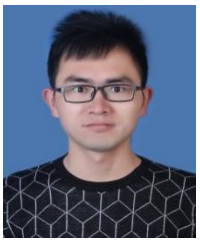

Sheng-Bing Shi was born in Hubei, China, in 1990. He received the B.S. degree in Physics from the Yangtze University, Jingzhou, China, in 2013. In 2015, he received the M.S. degree in Radio Physics at University of Electronic Science and Technology of China (UESTC). Currently, he is working toward the Ph.D. degree in Radio Physics at UESTC.

His research interest is computational electromagnetic.